Intra-Cavity Second-Harmonic Generation of Blue 460 nm Watt-Level Emission from Optically Pumped Semiconductor Disk Lasers

Frank Demaria and Alexander Hein

Experimental results with second-harmonic 460 nm-wavelength emission are presented. A profound analytical description of the intra-cavity beam shaping properties of the resonator based on the ABCD-law provides an effective design tool for the construction of appropriate resonator setups. Also described is the layer design of the optically pumped laser chip in which the fundamental radiation is generated. Overall conversion efficiencies up to 14.5 % and a maximum power of 1.6 W are demonstrated.

1. Introduction

High performance laser display applications require blue color light sources with a wavelength of 450–460 nm. Moreover, for this wavelengths a satisfying illuminance of reasonable large areas can only be provided by lasers with at least several hundred milliwatts of optical output power. Although laser diodes based on gallium nitride which are operating at wavelengths around 405 nm are suitable and frequently used laser sources for optical data storage, it still appears uncertain whether this approach leads to optical displays with the desired qualities. Here an alternative approach is described. The experimental results which are acquired by optically pumped semiconductor disk lasers in combination with intra-cavity second-harmonic-generation meet the mentioned demands.

2. Experimental Setup

Figure 1 shows a standard folded-cavity configuration which is commonly used for intra-cavity second-harmonic-generation (SHG) [1, 2]. In order to prevent absorption of the second harmonic in the semiconductor material, the critically phase-matched nonlinear crystal is localized in the outer resonator arm opposite to the laser chip. A 5 mm-long $3 \times 3\,\mathrm{mm}^2$ cross-section bismuth borate crystal (BiB_3O_3, BiBo) is used. The folding mirror and the external end mirror are designed to provide maximum reflectivity for the 920 nm fundamental radiation, but much lower reflectivity for the second harmonic with 460 nm wavelength. Wavelength stabilization, narrowing and tuning is realized by a 2 mm-thick birefringent quartz plate which is inserted under Brewster angle [3, 4]. The laser chip is mounted on a copper heat sink whose temperature is stabilized at a value of 0 °C by a Peltier cooler. Pump radiation from a fiber-coupled diode-laser is irradiated under an inclination angle of 30 ° with respect to the surface normal and focused to a spot-size of approximately $310\,\mu\mathrm{m} \times 270\,\mu\mathrm{m}$. The pump wavelength varies from 801 nm at threshold to 803 nm at the maximum pump power.

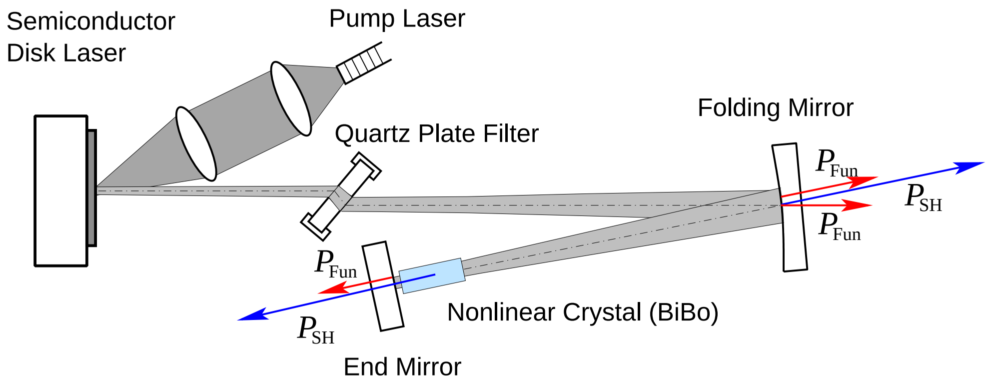

Fig. 1: Setup for second harmonic generation in a folded cavity configuration.

2.1 Analysis of beam and resonator

The design of a stable and effective resonator configuration is a challenging task. To provide high fundamental laser radiation, the laser chip has to be excited within a reasonable large area with diameters of several hundred micrometers. This defines the beam diameter of the laser mode at that position. On the other hand, the beam diameter in the outer resonator arm, where the nonlinear crystal is inserted, should be much smaller to achieve effective SHG. The distances between the mirrors should not be too big in order get an applicable and compact laser source with low aperture losses. Too small distances are also not desired in an easy to handle experimental setup with macroscopic components. Fortunately, with only few simplifying assumptions, a profound and clear analytical description of the resonator's beam shaping properties becomes possible. The influence of the laser chip on the beam propagation is neglected as well as the SHG crystal and the quartz-plate filter. According to fig. 2, the resonators geometry can be described

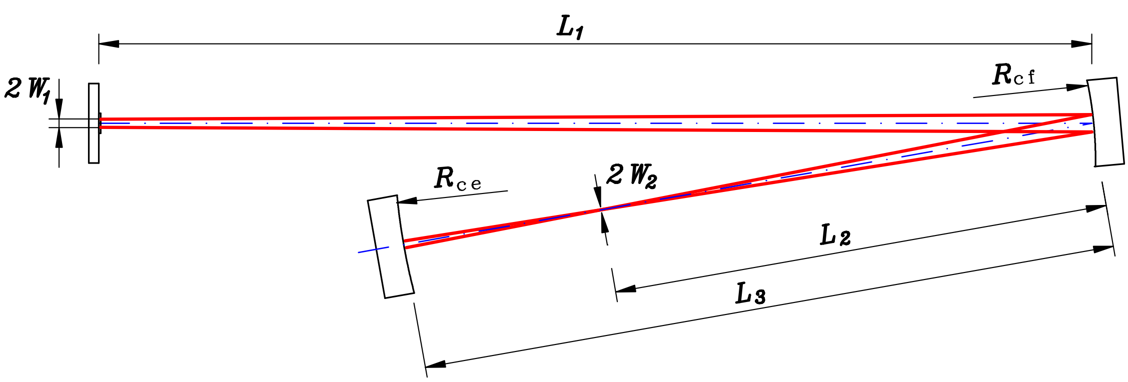

Fig. 2: Simplified geometry and parameters of the single-folded optical resonator setup with curved external mirrors.

by the distances L_1, L_3 and the radii of curvature R_{cf}, R_{ce} of the folding mirror and the end mirror. These parameters alone determine wether the resonator is stable or unstable. The approach for the theoretical description is the following. For a nondiffraction-limited optical beam, which is made up by a superposition of Laguerre–Gauss resonator modes, an effective radius of curvature of the phase fronts can be defined [7]. Stability of a linear resonator requires that the beam's effective radius of curvature at the end mirrors is identical with the radius of curvature of the end mirrors. One of them is the rear reflector of the laser chip. It is supposed to be plane. Thus, it is obvious that a beam waist is established inside the laser chip at the position of the rear reflector. Its diameter is assumed as $2W_1$. The second end mirror is the external end mirror which is realized by a multi-layer dielectrically-coated 0.5 inch-diameter glass substrate. The folding mirror is made up the same. For the shown configuration with a concave external end mirror, an external beam waist with the diameter $2W_2$ is located inside the outer resonator arm at a distance L_2 from the folding mirror. If a plane end mirror is used, the external beam waist is located at the surface of this mirror and L_3 becomes identical with L_2.

Paraxial ray analysis allows the simple description of the focussing characteristic of the mirrors by the focal length $f = R_\mathrm{c}/2$ and the ray transfer matrix formalism [8]. Finally, the resonator's caracteristical $ABCD$-matrix, given by the product of its single elementary transfer matrices has to be applied to the $ABCD$-law in order to derive analytical formula within the parametric description of Gaussian beams. The generalization to nondiffraction-limited beams with the wavelength λ and the beam waist radius W is implemented by the diffraction number M^2 and the definition of the Rayleigh range as

$$z_\mathrm{R} = \frac{\pi W^2}{M^2 \lambda} \tag{1}$$

[9]. Different Rayleigh ranges for the two resonator arms have to be considered. The Rayleigh ranges and beam waist positions are unambiguously determined by the resonators geometry. For a resonator with plane end mirrors ($L_2 = L_3$) and a folding mirror with a focal length $f_\mathrm{f} = R_\mathrm{cf}/2$ the spot-size reduction ratio

$$V = \frac{W_1}{W_2} \tag{2}$$

is given by

$$V = \sqrt{\frac{L_1 - f_\mathrm{f}}{L_2 - f_\mathrm{f}}} \tag{3}$$

and the chip-sided Rayleigh range by

$$z_\mathrm{R1} = V\sqrt{f_\mathrm{f}^2 - (L_1 - f_\mathrm{f})(L_2 - f_\mathrm{f})}. \tag{4}$$

For the more general case of a concave external end mirror with $f_\mathrm{e} = R_\mathrm{ce}/2$, the expression

$$z_\mathrm{R1}^2 = [f_\mathrm{f}^2 - (L_1 - f_\mathrm{f})(L_3 - f_\mathrm{f})] \frac{2f_\mathrm{e}(L_1 - f_\mathrm{f}) + f_\mathrm{f}^2 - (L_1 - f_\mathrm{f})(L_3 - f_\mathrm{f})}{2f_\mathrm{e}(L_3 - f_\mathrm{f}) - (L_3 - f_\mathrm{f})^2} \tag{5}$$

can be derived for the Rayleigh range [10]. In this case, the distance of the external beam waist from the folding mirror is determined by

$$L_2 = f_\mathrm{f}\, \frac{z_\mathrm{R1}^2 + L_1(L_1 - f_\mathrm{f})}{z_\mathrm{R1}^2 + (L_1 - f_\mathrm{f})^2} \tag{6}$$

and the spot-size reduction ratio can be calculated by expression (3) which is valid also for this case. Unlike the Rayleigh ranges and the spot sizes of the ideal Gaussian beam ($M^2 = 1$), the beam waists of the real beam with $M^2 > 1$ are underdetermined according to (1). Actually, it can be observed that the value of M^2 strongly depends on the spot-size of the pump beam on the laser chip for a given resonator configuration. That way an optimization of the overlap of the lateral beam intensity and the gain distribution of the laser chip takes place. The spot-size of the resulting beam is at any position M times lager than the embedded fundamental Gaussian mode which is generated by the same resonator. However, one restriction has to be considered. The beam waist diameters of the laser mode fit the size of the pumped area as long as they are significantly larger than the fundamental mode.

Best experimental results, concerning SHG output powers, have been achieved with a folding mirror with $R_{\mathrm{cf}} = 50\,\mathrm{mm}$ radius of curvature and an end mirror with $R_{\mathrm{ce}} = 1000\,\mathrm{mm}$, the latter could have been replaced by a plane mirror in principle. For each sample L_1 and L_3 have been adjusted to achieve maximum SHG output powers within the ranges 85–93 mm and 33–38 mm. The calculated parameters of the laser mode for such configurations can be taken from Fig. 3. The solid lines in the upper diagram show the mode diameters of the fundamental Gaussian mode on the laser chip. A pump-spot diameter with the same value leads to nearly fundamental mode operation. A larger pump spot leads to higher order modes which result in a larger effective diameter $2W_1$ of the laser mode and a higher M^2 value, which is illustrated as an example by the dashed line for $M^2 = 1.8$. The correlated external beam-waist diameter $2W_2$ and the reduction ratio V can be taken from the diagrams below. The bottom diagram shows the distance of the external beam-waist position from the end mirror which is negligible because of the high value of R_{ce}. Before the SHG-crystal is inserted, the resonator was adjusted to achieve stable and efficient fundamental laser operation. In this state, experimental investigations in which the diffraction number of the emitted beam is measured by a beam analyzer show very good agreement with theory. After the 5 mm long crystal is inserted, the external mirror has to be moved approximately 2 mm to enlarge the value of L_3. The enlargement is related to a shift of the (virtual) beam waist position. It can be quantified in a more detailled theoretical description that considers the length of the crystal and its effective refractive index. The same applies to L_1 and the birefringent filter.

2.2 Layer design of the disk laser chips

If the resonator is the framework of the laser setup, then the disk laser chip should be considered as the key component. Chips with different charcteristical features have been investigated. All structures are realized with a carefully elaborated layer design to provide high efficiencies and high optical output powers [5, 6].

Figure 4 shows a graphical representation of the top region of the investigated structure #1 with 6 single quantum wells. Its composition consists of a dielectric surface layer, a resonant periodic gain structure and the rear double-band Bragg reflector (DBBR). The DBBR is designed to provide high reflectivity not only for the fundamental lasing wavelength but also for the incident pump light. Thus, it has to be considered that the

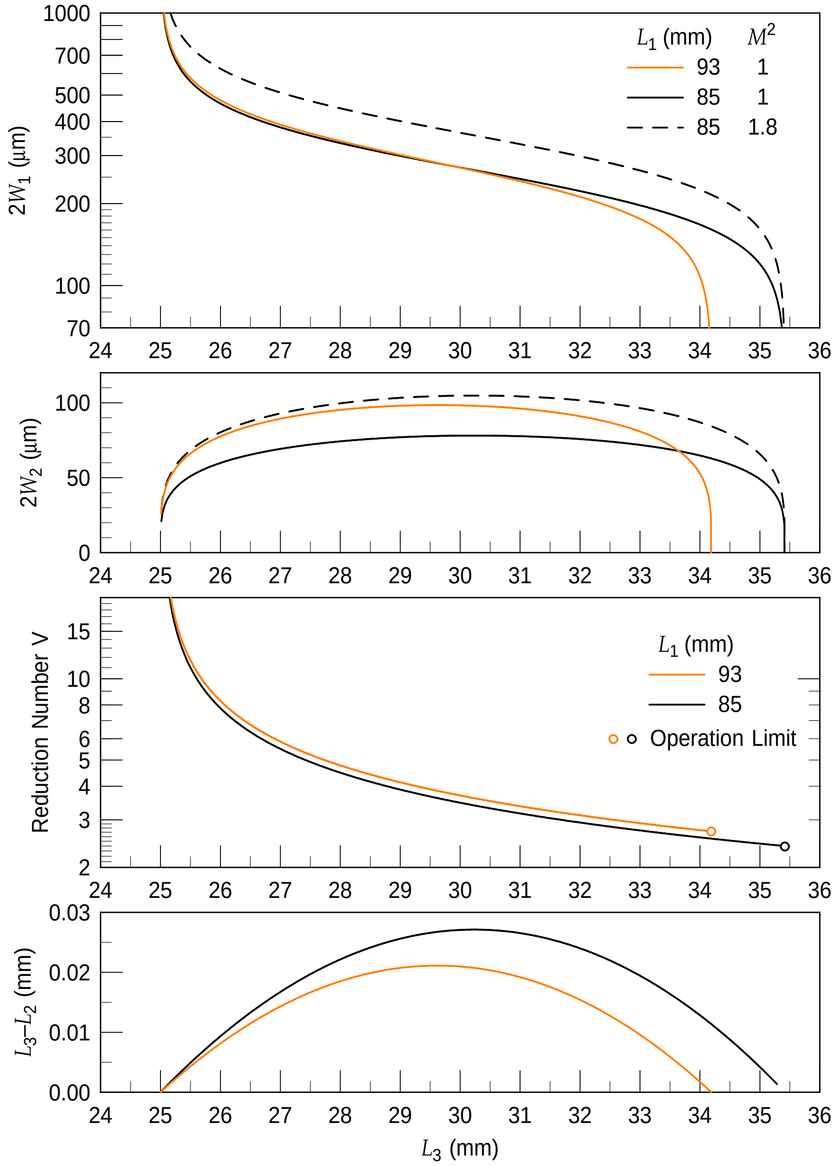

Fig. 3: Calculated relations of the resonator's geometrical parameters for a folding mirror with $R_{\mathrm{cf}} = 50\,\mathrm{mm}$ and an end mirror with $R_{\mathrm{ce}} = 1000\,\mathrm{mm}$. From top to bottom: laser-mode spot size on the chip, spot size of the external focus, spot-size reduction ratio, distance of external focus from the end mirror.

longitudinal field distribution of the pump light inside the structure is much more dominated by a standing wave than by an exponential decrease that results from absorption. The 84 nm-thick TiO_2 surface layer with a refractive index of 2.381 for the pump wavelength is designed to lower the surface reflectivity to a value of 5.4 % for an unpolarized beam which is irradiated under 30°. That way, maximum absorbance values around 95 % can be achieved. Furthermore, the contrast of the refractive indexes is much higher at the interface to air than at the interface to the semiconductor layers. Therefore a maximum of the resonant pump field is located at this position and a minimum nearby the interface to the semiconductor structure inside the absorbing 5 nm-thick GaAs anti-oxidation

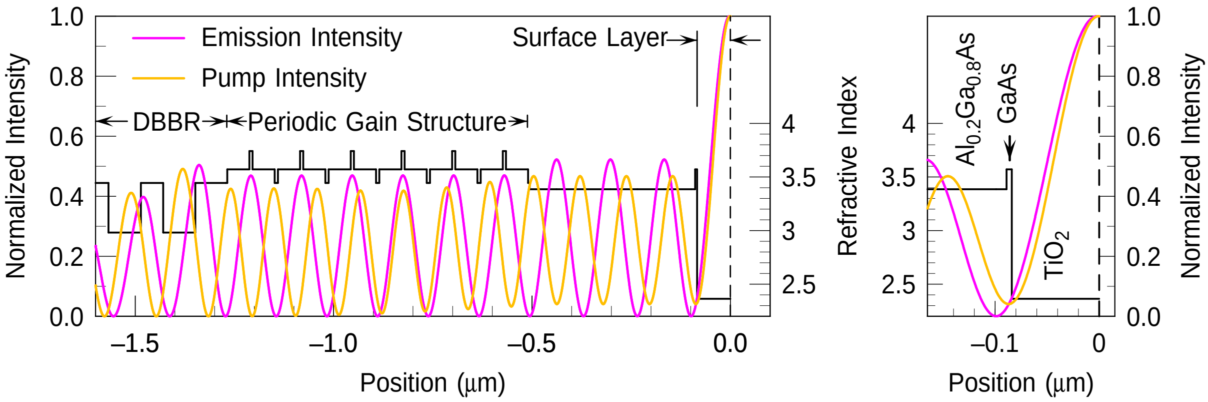

Fig. 4: Top region of structure #1, visualized by the index of refraction, beginning from the surface layer to the first layers of the DBBR (left). Also shown are both calculated electric field intensities for the emission wavelength $\lambda_e = 920\,\mathrm{nm}$ and the pump wavelength $\lambda_e = 803\,\mathrm{nm}$ with an angle of incidence $\theta_i = 30°$. In detail shown is the junction between the dielectric surface layer and the underlying semiconductor layers where nodes of the electric field intensities are located (right).

layer. This layer is necessary to protect the underlying aluminum containing material during the fabrication process. The gain structure is formed by a periodic sequence of several 8 nm-thick $In_{0.08}Ga_{0.92}As$ quantum wells which are surrounded by GaAs barriers. Number and type of the quantum wells of the different samples are given in table 1. The

Table 1: Caracteristical features of the laser-chip samples.

Sample	Quantum wells	Distance from wafer center
#1a	6 single	8 mm
#1b	6 single	8.5 mm
#2	8 double	2 mm

periods of quantum wells with their surrounding barriers are separated by $GaAs_{0.71}P_{0.29}$ strain compensation layers [3, 11] which also act as a carrier diffusion barrier. The double quantum wells of structure #2 contain a 10 nm-thick intermediate GaAs barrier.

3. Second-Harmonic Output Characteristics

Figure 5 shows an overview of the output characteristics for three laser chips with the best performance. The output powers where limited by the cooling capacity of the Peltier thermoelectric device that was used for temperature stabilization. For all measurements, the orientation of the critical phase matched crystal was adjusted for maximum output power at the highest pump power. The best performance is achieved with sample #1a, a structure with 6 single quantum wells. At an incident pump radiation of 11 W a SHG output power of 1.6 W is measured which results in an overall conversion efficiency of

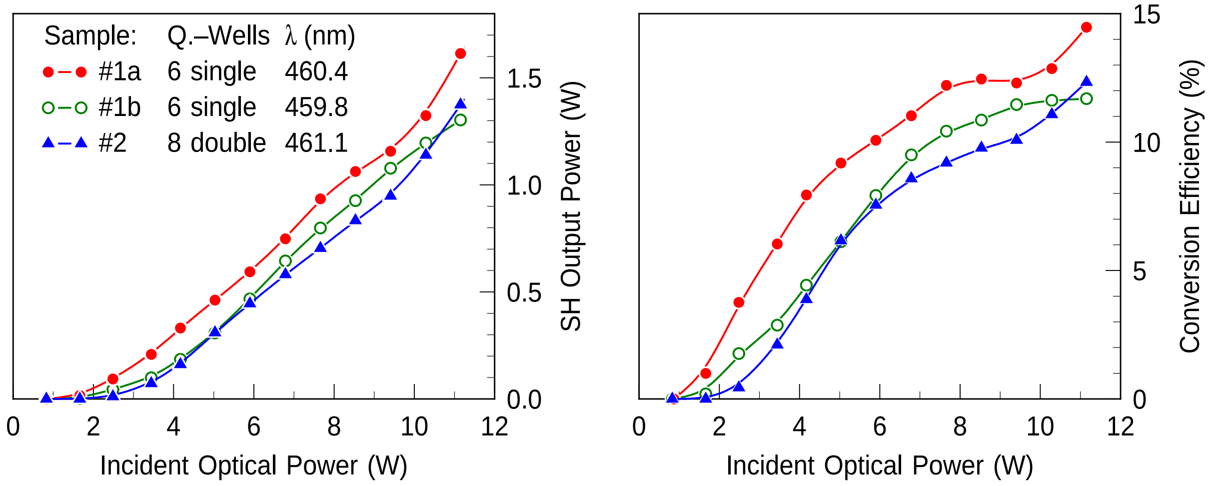

Fig. 5: Second harmonic optput power characteristics (left) and the corresponding overall conversion efficiency (right).

14.5 %. The fundamental radiation was filtered out with an optical band-edge filter. A 10 dB spectral linewidth of about 2.6 nm is typically observed as shown in the spectrum in fig. 6.

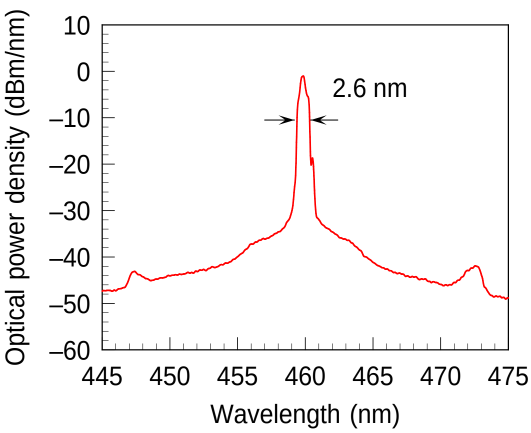

Fig. 6: Typical spectrum of the second harmonic taken from sample #1b. The linewidth at the 10 dB drop is 2.6 nm.

4. Conclusion and Outlook

The described combination of an optically pumped semiconductor disk laser with a nonlinear crystal in a folded resonator may appear complex and extensive. It has been demonstrated however, that the utilization of properly designed and fabricated laser chips in an adequate resonator configuration leads to a blue laser source with unique properties. The given analytical equations which realistically describe the beam shaping properties of the resonator are quite useful for the dimensioning of stable resonator conifgurations for efficient intra-cavity second-harmonic-generation. The maximum output power was limited by thermal roll over arising from insufficient heat removal. Only simple copper heat spreaders and customized peltier coolers have been utilized for the experiments. Because of its nonlinear nature, the generation of the second harmonic becomes more efficient with increasing intensity of the fundamental radiation. It seems that the utilization of diamond heat spreaders with much better thermal conductivity and Peltier devices with higher cooling capacity can lead to even brighter, multi-watt level laser sources.

References

[1] M. Fallahi, L. Fan, Y. Kaneda, C. Hessenius, J. Hader, H. Li, J. Moloney, B. Kunert, W. Stolz, S. Koch, J. Murray, and R. Bedford, "5-W yellow laser by intracavity frequency doubling of high-power vertical-external-cavity surface-emitting laser", *IEEE Photon. Technol. Lett.*, vol. 20, no. 20, pp. 1700–1702, 2008.

[2] J.Y. Kim, S. Cho, S.-J. Lim, J. Yoo, G.B. Kim, K.-S. Kim, J. Lee, S.-M Lee, T. Kim, and Y. Park, "Efficient blue lasers based on gain structure optimizing of vertical-external-cavity surface-emitting laser with second harmonic generation", *J. Appl. Phys.*, vol. 101, no. 3, pp. 033103-1–4, 2007.

[3] J.W. Evans, "The birefringent filter", *J. Opt. Soc. Am.*, vol. 39, no. 3, p. 229, 1949.

[4] M. Jacquemet, M. Domenech, G. Lucas-Leclin, P. Georges, J. Dion, M. Strassner, I. Sagnes, and A. Garnache, "Single-frequency cw vertical external cavity surface emitting semiconductor laser at 1003 nm and 501 nm by intracavity frequency doubling", *Appl. Phys. B*, vol. 86, pp. 503–510, 2007.

[5] F. Demaria, S. Lorch, S. Menzel, M. C. Riedl, F. Rinaldi, R. Rösch, and P. Unger, "Design of highly efficient high-power optically pumped semiconductor disk lasers", *IEEE J. Select. Topics Quantum Electron.*, vol. 15, no. 3, pp. 973–977, 2009.

[6] F. Demaria, "Layer Design of Highly Efficient Optically Pumped Semiconductor Disk Lasers", *Annual Report 2008*, pp. 41–48. Ulm University, Institute of Optoelectronics.

[7] A. E. Siegman, "Defining the Effective Radius of Curvature for a Nonideal Optical Beam", *IEEE J. Quantum Electron.*, vol. 27, no. 5, pp. 1146–1148, 1991.

[8] H. Kogelnik and T. Li, "Laser beams and resonators", *Appl. Opt.*, vol. 5, no. 10, pp. 1550–1567, 1966.

[9] P. A. Bélanger, "Beam propagation and the ABCD ray matrices", *Opt. Lett.*, vol. 16, no. 14, pp. 196–198, 1991.

[10] F. Demaria, *Schicht und Resonatordesign von Halbleiterscheibenlasern*. Ph.D. thesis, Ulm University, Ulm, Germany, 2008.

[11] F. Rinaldi, "Advanced Strain Compensation in MBE Grown Semiconductor Disk Lasers", *Annual Report 2009*, pp. 11–15. Ulm University, Institute of Optoelectronics.

[12] F. Rinaldi, *MBE Growth and Characterization of Multilayer Structures for Vertically Emitting Laser Devices*. Ph.D. thesis, URL: http://vts.uni-ulm.de/doc.asp?id=6667, Ulm University, Ulm, 2008.